

Quantum wire networks with local \mathbb{Z}_2 symmetry

K. Kazymyrenko,^{1,*} S. Dusuel,^{2,†} and B. Douçot^{1,‡}

¹*Laboratoire de Physique Théorique et Hautes Energies,
CNRS UMR 7589, Université Paris VI et VII,
4, Place Jussieu, 75252 Paris Cedex 05, France*

²*Institut für Theoretische Physik, Universität zu Köln, Zülpicher Str. 77, 50937 Köln, Germany*

For a large class of networks made of connected loops, in the presence of an external magnetic field of half flux quantum per loop, we show the existence of a large local symmetry group, generated by simultaneous flips of the electronic current in all the loops adjacent to a given node. Using an ultra-localized single particle basis adapted to this local \mathbb{Z}_2 symmetry, we show that it is preserved by a large class of interaction potentials. As a main physical consequence, the only allowed tunneling processes in such networks are induced by electron-electron interactions and involve a simultaneous hop of two electrons. Using a mean-field picture and then a more systematic renormalization-group treatment, we show that these pair hopping processes do not generate a superconducting instability, but they destroy the Luttinger liquid behavior in the links, giving rise at low energy to a strongly correlated spin-density-wave state.

PACS numbers: 71.10.Li, 71.10.Pm, 73.21.Hb

I. INTRODUCTION

For the past two decades, transport properties of quantum wires have received a lot of attention^{1,2}. Besides metallic systems, two dimensional electron gases induced in GaAs/AlGaAs heterostructures have displayed a rich variety of quantum effects such as Aharonov-Bohm resistance oscillations in a ring geometry^{3,4}, and persistent currents^{5,6}. More recently, coherent Aharonov-Bohm oscillations have been measured in ballistic arrays with the dice lattice geometry⁷, in agreement with the predictions of simple models for non-interacting electrons⁸. The experimental visibility of conductance oscillations with the full flux quantum $\Phi_0 = h/e$ periodicity in large structures with a few thousand loops has been attributed to the presence of Aharonov-Bohm cages which localize the motion of electrons when the external flux per elementary loop is half-integer in units of Φ_0 .

After these first investigations, a natural issue is to understand interaction effects on this geometrical localization phenomenon. For two electrons, it was shown that interaction induces some correlated hopping processes, at the origin of some delocalized states in which the two electrons always remain close from each other^{9,10}. Remarkably, this trend appears for any sign of interaction. Of course, for a repulsive interaction, these extended states lie above the ground-state sector, obtained when the two electrons are individually localized in distinct remote cages. But this raises the question of what happens at finite density, where it is no longer possible to put all conduction electrons in separate cages. Two electrons initially in the same cage will be able to move together, so this may generate some kind of metallic state.

An interacting system with a finite particle density was first studied in its *bosonic* version in a one-dimensional geometry showing Aharonov-Bohm cages, namely a chain of rhombi¹¹. This model has been adapted into a realistic description of a Josephson junction array with the

same geometry recently¹². There, it was found that no single boson condensate can exist, but instead a 2-boson condensate is stabilized at low energy. This peculiar phenomenon is connected to the single particle localization in Aharonov-Bohm cages, but in the presence of interaction, it requires a stronger property, identified as a local symmetry based on the \mathbb{Z}_2 group. This symmetry implies that the parity of the total particle number within any Aharonov-Bohm cage is conserved. If this symmetry remains unbroken, it prevents the formation of any single boson condensate. A two-dimensional version exhibiting this local \mathbb{Z}_2 symmetry was also analyzed¹³, in the context of topologically protected quantum memories. The crucial role of a local symmetry is well illustrated by the example of the dice lattice, which sustains Aharonov-Bohm cages, but no local symmetry in the presence of interactions. There, it was found that the external magnetic field corresponding to $\Phi_0/2$ per loop imposes a vortex lattice which allows for some zero-energy line defects, but the single particle condensate exhibits a finite phase stiffness^{14,15,16}.

The fermionic case at finite density is the subject of the present article. Motivated by ongoing experiments¹⁷ on networks designed on a 2D electron system at a GaAs/GaAlAs interface, we shall study quantum wire networks, which geometry is compatible with a local \mathbb{Z}_2 symmetry in the presence of a magnetic field of half flux quantum per elementary loop. Such networks will be called \mathbb{Z}_2 networks, and two examples are shown on Fig. 1 below. In section II, we define precisely this class of networks, construct the unitary operators associated to the local \mathbb{Z}_2 symmetry group, and consider their irreducible representations in the Hilbert space of a single particle. We show that all the common eigenstates of all the local generators of this large Abelian group are strongly localized within Aharonov-Bohm cages involving only a finite number of elementary loops. Section III first discusses the matrix elements of a two-body interaction in

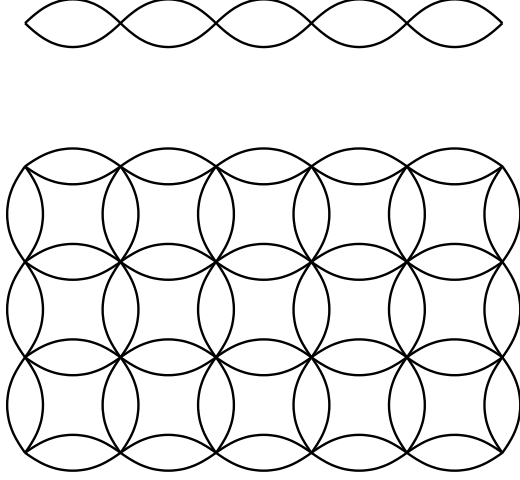


FIG. 1: This picture presents two examples of \mathbb{Z}_2 networks: a chain of loops (upper part), and a square lattice of loops (lower part). All these networks are obtained from any planar lattice after replacing each link by a loop. To get a local \mathbb{Z}_2 symmetry, each loop is required to be perfectly invariant under the reflection through the long axis defined by its two adjacent nodes.

this localized basis adapted to the \mathbb{Z}_2 symmetry. This shows that a large class of pair interaction potentials (including the point-like Hubbard interaction) is compatible with this symmetry. We then show that, at least in a mean-field approach, the particle pair hopping processes generated by a repulsive interaction do not lead to superconductivity. Starting from simple order of magnitude estimates adapted to semi-conductor quantum wire networks, we argue that a more refined renormalization group approach (RG) is required, given the strength of the Coulomb interaction for typical electronic densities. Finally, section IV proposes a simplified \mathbb{Z}_2 symmetric model of coupled Aharonov-Bohm cages which is analyzed with the RG method using the one-loop approximation. This confirms the irrelevance of the electron pair hopping processes in the low-energy limit, and establishes a tendency for the system to reach a strong coupling fixed point of a spin density wave character. So the combination of local \mathbb{Z}_2 symmetry and electron-electron repulsion destroys the Luttinger liquid in the quantum wires which constitute the network, leaving room only for a strongly correlated liquid with mostly gapped excitations. Finally, a brief appendix shows how this picture fits with a simple mean-field description.

II. LOCAL \mathbb{Z}_2 SYMMETRY FOR A CLASS OF QUANTUM NETWORKS

A. Basic construction

In this paper, we shall consider networks of quantum wires (called \mathbb{Z}_2 networks), for which the elementary links

connecting two nearest-neighbor nodes are doubled. In other words, such networks may be obtained from any planar graph, after replacing links by loops. Examples of this construction are shown on Fig. 1. The key assumption we shall make is that all these loops exhibit a perfect reflection symmetry around the axis joining the two nodes connected by the loop. This requirement imposes some rather severe constraints on the fabrication of such structures, in terms of the network geometry, and of the control of various types of disorder. However, as discussed in the Introduction, experimental observation of the Aharonov-Bohm cage effect in GaAs quantum wire networks⁷ suggests that present technology is able to meet these constraints. On a more theoretical side, numerical investigations on disordered tight-binding versions of such networks have shown that the effects we shall discuss survive after a small but sizeable disorder is introduced¹⁰. At a purely geometric level, these structures exhibit, besides their usual crystalline symmetry groups, a large symmetry generated by local flips of elementary loops around their central axis. We are mostly addressing here the quantum-mechanical effects of such a symmetry in the presence of a constant and uniform external magnetic field, corresponding to half-flux quantum per loop.

As usual, quantum mechanics is affected by the fact that the vector potential used to describe the magnetic field is not invariant under these local operations. In the case of the translational symmetry, this leads to the non-commutation of magnetic translations and to Landau level quantization. In the present case, the striking consequence is the appearance of a dramatic localization phenomenon, where all single particle energy eigenstates are confined inside a finite set of loops⁸.

To illustrate the idea, it is useful to consider first a single loop, with strictly one-dimensional motion along a coordinate x . If l denotes the perimeter of this loop, we have to impose the periodicity condition: $\psi(l) = \psi(0)$. The stationary Schrödinger equation reads:

$$E\psi(x) = \frac{1}{2m}(\hat{p} + eA)^2\psi(x) = \frac{1}{2m}(-i\hbar\frac{d}{dx} + eA)^2\psi(x)$$

where $A(x)$ is the projection of the vector potential along the wire at point x . Using the gauge transformation: $\psi(x) = \exp(-i\frac{e}{\hbar}\int_0^x A(x')dx')\chi(x)$, $\chi(x)$ obeys the Schrödinger equation for a free particle, subjected to the boundary condition: $\chi(l) = \exp(i2\pi\Phi/\Phi_0)\chi(0)$, where $\Phi = \frac{e}{\hbar}\int_0^l A(x')dx'$ is the magnetic flux through the loop and $\Phi_0 = h/e$ is the flux quantum. The single particle energy spectrum is then: $E_n = \frac{2\pi^2\hbar^2}{ml^2}(n + \Phi/\Phi_0)^2$, where n is any integer. For generic values of Φ/Φ_0 , all energy eigenvalues are non-degenerate, but all levels are doubly degenerate when $2\Phi/\Phi_0$ is an integer (with the exception of the ground-state for integer Φ/Φ_0). For integer Φ/Φ_0 , the flux through the loop may be eliminated by a gauge transformation, and the degeneracy is clearly attributed to the reflection symmetry, which changes the wave-number of an eigenstate into its opposite. In the case

of half-integer Φ/Φ_0 , this geometrical symmetry has to be combined with a gauge transformation so that $\psi(x)$ is changed into $(T\psi)(x) \equiv \psi'(x) = \exp(if(x))\psi(-x)$, with $f(x) = \frac{e}{\hbar} \left(\int_0^{-x} A(x')dx' - \int_0^x A(x')dx' \right)$. This transformation sends an eigenstate with a persistent current into an eigenstate with the reversed current. We also notice that $\psi'(0) = \psi(0)$ whereas $\psi'(l/2) = -\psi(l/2)$. This has some important consequences if we wish to generalize these reflection operations to the elementary loops connecting nodes in \mathbb{Z}_2 networks.

Let us first consider a one dimensional chain of loops, as shown on the upper part of Fig. 1. Any link of this chain can be represented by a simple line with plus and minus signs on its extremities, see Fig. 2, reminding us the sign of the transformed wavefunction. Suppose now we try to construct a symmetry associated to the reflection for just one loop. The simplest way is to combine as before reflection and gauge transformation, but we encounter a major problem: this transformation will be no longer local, because we are obliged to change globally the sign of the part of the wave-function lying on one side of the transformed loop. For an open chain, this non local aspect of the transformation attached to a single loop is not too disturbing, since it modifies physical observables such as electronic current only locally. But in the case of periodic boundary conditions, it has the consequence that such a transformation simply becomes impossible. In fact, one can easily avoid this difficulty by considering two transformations on adjacent loops, see Fig. 2. The generalization for any \mathbb{Z}_2 lattice is clear, we need to join together negative extremities of all the loops arriving at a given node. Because of these phase-factors arising from gauge transformations, the local symmetry generators are therefore associated to lattice *sites* and not to the *links* as one would infer from purely geometrical considerations. Note that in lattice gauge theories, local generators of gauge transformations are also attached to lattice sites, which establishes a close connection between \mathbb{Z}_2 networks and lattice gauge theories based on the \mathbb{Z}_2 group. This viewpoint has been emphasized in the context of Josephson junction arrays^{18,19}.

In case of an *integer* number of flux quanta per loop ($\Phi = n\Phi_0$), we have now $\psi'(0) = \psi(0)$ and $\psi'(l/2) = \psi(l/2)$, so that each link carries plus signs on both ends. In this case, it is possible to construct local \mathbb{Z}_2 symmetry generators associated to lattice *links* instead of nodes. But then, because the single particle Hamiltonian has mostly a dispersive spectrum, simultaneous eigenstates of the Hamiltonian and these local generators are extended, instead of being localized as in the half-flux case.

B. Constraints on scattering matrices at the nodes

Let us now describe more precisely the local transformation attached to a given site i on a \mathbb{Z}_2 network. This site belongs to n elementary loops, so it is the intersec-

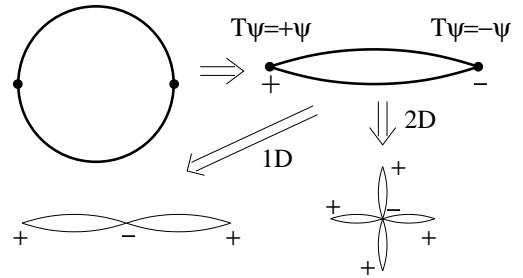


FIG. 2: This picture shows different realizations of a local \mathbb{Z}_2 symmetry, successively for a single loop (upper part), and then around sites present in a 1D geometry (chain of loops, lower left) or a 2D geometry (square lattice of nodes connected by loops, lower right). Signs plus or minus keep track of the relative sign between initial and transformed wavefunctions ψ and $T\psi \equiv \psi'$.

tion of $2n$ links. Since these links are naturally paired, we shall label them by a compound index $(ij\alpha)$, where j refers to any of the n nearest neighbors of site i , and $\alpha \in \{1, 2\}$. On each of these $2n$ links, we choose the origin of an x coordinate at site i , and the projection of the local vector potential along this link is denoted by $A_{ij\alpha}(x)$. As already discussed, it is convenient to write the single-particle wave-function as:

$$\psi_{ij\alpha}(x) = \exp \left(-i \frac{e}{\hbar} \int_0^x A_{ij\alpha}(x')dx' \right) \chi_{ij\alpha}(x)$$

along the link $(ij\alpha)$, where an eigenstate with energy $E = \frac{\hbar^2 k^2}{2m}$ has the form:

$$\chi_{ij\alpha}(x) = C_{ij\alpha} e^{-ikx} + D_{ij\alpha} e^{ikx}$$

Here, $C_{ij\alpha}$ (resp. $D_{ij\alpha}$) is the amplitude of an incoming (resp. outgoing) wave with respect to site i . Since $\chi_{ij\alpha}(x)$ is locally the wave-function of a free particle with no magnetic field, we may define in a gauge-invariant way a scattering matrix at site i by:

$$D_{ij\alpha} = \sum_{j'\alpha'}^{(i)} S_{j\alpha, j'\alpha'}^{(i)} C_{ij'\alpha'} \quad (1)$$

which expresses outgoing amplitudes as a function of incoming ones. Using the notation $\bar{1} = 2$ and $\bar{2} = 1$, the local \mathbb{Z}_2 generators commutes at any site with the single particle Hamiltonian if and only if:

$$S_{j\bar{\alpha}, j'\alpha'}^{(i)} = S_{j\alpha, j'\alpha'}^{(i)} = S_{j\alpha, j'\bar{\alpha}'}^{(i)} \quad (j \neq j') \quad (2)$$

$$S_{j\bar{\alpha}, j\bar{\alpha}'}^{(i)} = S_{j\alpha, j\alpha'}^{(i)} \quad (3)$$

where i denotes any site, and j, j' are arbitrary nearest neighbors of i . In other words, there should be a perfect symmetry between paired links $ij\alpha$ and $ij\bar{\alpha}$. The proof of this rather intuitive statement will be given in the next paragraph. Note that in real systems, nodes always have a finite area, and this constraint may be difficult to

implement. For instance, as shown on Fig. 3, in a chain of loops, it seems very likely that the simplest design for a node does not satisfy this symmetry. A suggestion for improving this local geometry is sketched on the bottom of Fig. 3. Generalizations to multichannel quantum wires are possible, if the underlying inversion symmetry is also performed on the transverse channels. But we have to restrict ourselves to a regime of weak magnetic fields so that we may neglect the field effects on orbital motion within a wire.

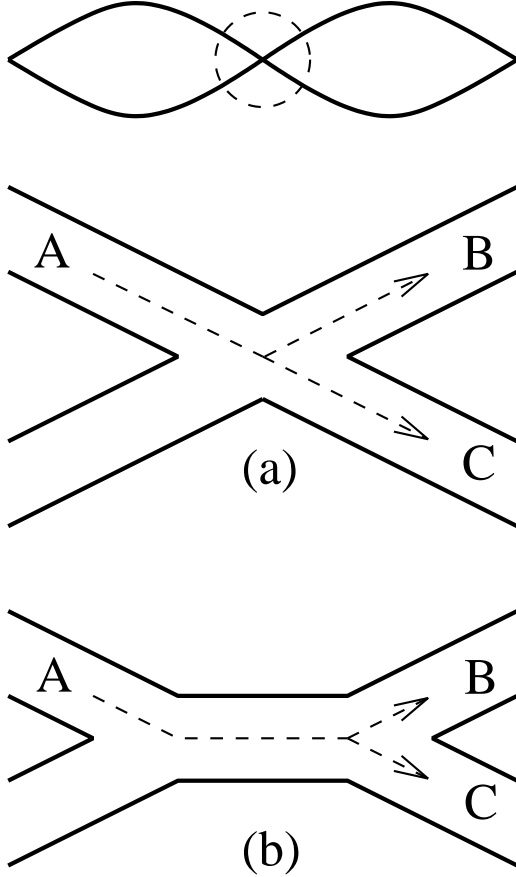


FIG. 3: This picture illustrates the requirements on the scattering matrix at a node present in a chain of loops (upper part), in order to impose a local \mathbb{Z}_2 symmetry. The most direct design (a), is likely to be incompatible with these constraints, since intuitively, the amplitude for an electron to go from A to B is different from the amplitude to go from A to C. In a slightly modified design (b), these amplitudes are more likely to be equal, and this is more appropriate for an experimental implementation of the local \mathbb{Z}_2 symmetry.

Let us now check that conditions (2),(3) are all we need. The transformation attached to site i now reads:

$$\begin{aligned} \psi'_{ij\alpha}(x) = & \quad (4) \\ & - \exp \left(i\sigma_\alpha \frac{e}{\hbar} \int_0^x (A_{ij2}(x') - A_{ij1}(x')) dx' \right) \psi_{ij\bar{\alpha}}(x) \end{aligned}$$

where $\sigma_1 = 1$ and $\sigma_2 = -1$. Using the locally gauge-invariant description in terms of $\chi_{ij\alpha}(x)$, this trans-

lates into: $\chi'_{ij\alpha}(x) = -\chi_{ij\bar{\alpha}}(x)$, which is equivalent to $C'_{ij\alpha} = -C_{ij\bar{\alpha}}$, and $D'_{ij\alpha} = -D_{ij\bar{\alpha}}$. This operation leaves the S matrix at site i invariant if and only if:

$$S_{j\bar{\alpha}, j'\bar{\alpha}'}^{(i)} = S_{j\alpha, j'\alpha'}^{(i)} \quad (5)$$

Note that this is valid for any j and j' which are nearest neighbors of i . When $j = j'$, we recover condition (3), and when $j \neq j'$, it is implied by condition (2). But we should also check that the transformation attached to site i also preserves the S matrix at all nearest-neighbor sites j of i . Along the link $ij\alpha$, we have to perform a change of origin, permuting i and j , and replacing x by $y = l_{ij} - x$, where l_{ij} is the common length of the two links ($ij1$) and ($ij2$). Using the fact that the flux through the loop enclosed by these two links is half a flux quantum modulo Φ_0 , Eq. (4) becomes:

$$\begin{aligned} \psi'_{ji\alpha}(y) = & \quad (6) \\ & \exp \left(i\sigma_\alpha \frac{e}{\hbar} \int_0^y (A_{ji2}(y') - A_{ji1}(y')) dy' \right) \psi_{ji\bar{\alpha}}(y) \end{aligned}$$

which implies $\chi'_{ji\alpha}(x) = \chi_{ji\bar{\alpha}}(x)$, or: $C'_{ji\alpha} = C_{ji\bar{\alpha}}$, and $D'_{ji\alpha} = D_{ji\bar{\alpha}}$. This yields $S_{i\bar{\alpha}, i\bar{\alpha}'}^{(j)} = S_{i\alpha, i\alpha'}^{(j)}$, that is Eq. (3) after a permutation of i and j . Now, for any site j' , nearest neighbor of j and distinct from i , the transformation based at site i does not affect the pair of links $(jj'\alpha)$, so $C'_{jj'\alpha} = C_{jj'\alpha}$, and $D'_{jj'\alpha} = D_{jj'\alpha}$, which implies $S_{i\bar{\alpha}, j'\alpha'}^{(j)} = S_{i\alpha, j'\alpha'}^{(j)}$ and $S_{j'\bar{\alpha}', i\bar{\alpha}}^{(j)} = S_{j'\alpha', i\alpha}^{(j)}$, that is Eq. (2) after a permutation of i and j .

C. Irreducible representations of local \mathbb{Z}_2 symmetry

Let us denote by U_i the unitary transformation attached at site i , defined by Eq. (4). Clearly, $U_i^2 = \mathbf{1}$, so the eigenvalues of U_i are ± 1 . Furthermore, it is simple to check that U_i and U_j commute. The only non-trivial case arises when i and j are nearest neighbors. In fact, comparing Eqs. (4) and (6) we see that the actions of U_i and U_j on the loop between i and j differ only by a sign. The mutual commutation of these operators ensures that they can be simultaneously diagonalized, so that $U_i|\Psi\rangle = \epsilon_i|\Psi\rangle$, with $\epsilon_i = \pm 1$. For single particle states, the possible collections of eigenvalues $\{\epsilon_i\}$ are very limited. To identify them, we need to introduce the notion of an Aharonov-Bohm cage. For any lattice site i , the cage attached to i is composed of all the elementary loops which contain i . We have now the following properties:

Property (a): If i and j are nearest-neighbor sites, and if $U_i|\Psi\rangle = U_j|\Psi\rangle$, then the wave-function associated to $|\Psi\rangle$ vanishes on the loop joining i and j .

This is an immediate consequence of the fact that along this loop, $U_i|\Psi\rangle$ and $U_j|\Psi\rangle$ are described by opposite wave-functions, as already noted (compare Eqs. (4) and (6)).

Property (b): If $U_i|\Psi\rangle = -|\Psi\rangle$, the wave-function ψ attached to $|\Psi\rangle$ vanishes everywhere outside the Aharonov-Bohm cage attached to i .

This follows directly from the fact that the transformation U_i does not modify the wave-function outside the Aharonov-Bohm cage attached to i .

Main Property: The only possible collections of simultaneous eigenvalues $\{\epsilon_i\}$ are such that exactly one of them is equal to -1 , all the others being equal to 1 . If i is the only site with $\epsilon_i = -1$, the corresponding wave-function vanishes everywhere outside the Aharonov-Bohm cage attached to i .

Because of property (a), if all ϵ_i 's are equal to 1 , $|\Psi\rangle$ vanishes. So at least one eigenvalue is negative. Suppose we have two of them: $\epsilon_i = \epsilon_j = -1$ with $i \neq j$. Because of property (b), the wave-function ψ vanishes everywhere outside the intersection of the cages centered at i and j . If this intersection is empty, then $|\Psi\rangle = 0$. If not, then i and j are nearest neighbors. But then, property (a) implies that ψ vanishes also on the loop joining i and j , so $|\Psi\rangle = 0$. The only possibility is therefore to have $\epsilon_i = -1$ and $\epsilon_j = 1$ for any $j \neq i$. From property (b), the wave-function is confined inside the Aharonov-Bohm cage centered around site i .

When the S matrix of each node satisfies conditions (2) and (3) for any wave-vector k , we may diagonalize the single-particle Hamiltonian in a localized basis of Aharonov-Bohm cage wave-functions. Since each of these cages has only a finite total wire length, the energy spectrum is always discrete. These cages behave as artificial atoms, at least as long as electrons are not interacting. The interesting feature of such a system is that two cages may overlap, which allows for non-trivial interaction effects.

All these results (for $\Phi = \Phi_0/2$) have a simple physical interpretation in the light of the Aharonov-Bohm effect. Suppose we have an electron situated at a node i . If j is a nearest-neighbor of i , there are two possible equivalent ways for this electron to reach a nearby loop (j, k) , using either side of loop (i, j) . But the associated probability amplitudes have opposite signs (as $\exp(i2\pi\Phi/\Phi_0) = -1$) and will compensate each other. This is why we obtain localized solutions which form a complete basis of the Hilbert space for non-interacting electrons.

In case of integer number of flux quanta per loop, the functions within a given irreducible representation are not necessarily local, so the previous conclusions do not apply. It happens that some localized solutions still exist, but they form only “half” of a complete basis of states. This analysis could be made using the Kottos and Smilansky formalism²⁰, but to save space and since we are mostly interested in half-flux quantum per loop, we will not give further detail on the integer flux case in this paper.

III. INTERACTION EFFECTS ON AHARONOV-BOHM CAGES

A. Hamiltonian for interacting electrons in an Aharonov-Bohm cage basis

In the case of interacting electrons, this simple physical picture has to be deeply modified, because the two sides of a given loop are no longer equivalent if an electron “sees” on one of them another electron and interacts with it. So the probability for one electron to hop from an Aharonov-Bohm cage to a nearby one no longer vanishes. However, this is an interaction-induced effective hopping, and it is by no means obvious that it could lead to a coherent metallic system in the usual sense. By contrast to lattices such as the dice lattice which also exhibit the Aharonov-Bohm cage phenomenon, we will now show that on \mathbb{Z}_2 lattices, and for a large class of electron-electron interactions, the local \mathbb{Z}_2 symmetry is still present. This puts some rather severe constraints on the amount of delocalization that interactions may induce for a finite density of electrons. Because of the local \mathbb{Z}_2 symmetry, only *pairs* of electrons are able to hop from one cage to an adjacent one. So on intuitive grounds, a true conducting state is expected only for attractive interactions, where it is also a superconductor. For repulsive interactions, we shall see that the system remains an incoherent metal.

For the sake of simplicity, we shall consider here a local Hubbard repulsive interaction between electrons. Generalization to a large class of interaction potentials is given in Section III B below. This interaction may be written as:

$$H_{\text{int}} = U \sum_{ij\alpha} \int_0^{l_{ij}} dx \psi_{ij\alpha\uparrow}^\dagger(x) \psi_{ij\alpha\downarrow}^\dagger(x) \psi_{ij\alpha\downarrow}(x) \psi_{ij\alpha\uparrow}(x) \quad (7)$$

Here $\psi_{ij\alpha\uparrow}^\dagger(x)$ is the second quantization electron creation operator at point x on the wire $\alpha = \{1, 2\}$ joining nodes i and j , with spin projection \uparrow along the quantization axis. Let us now introduce operators of creation and annihilation of an electron in a given Aharonov-Bohm cage state: $c_{i\tau}^\dagger(x)$ and $c_{i\tau}(x)$ respectively, τ referring to the spin projection. They satisfy the following relations:

$$U_i c_{i\tau}^\dagger(x) U_i = -c_{i\tau}^\dagger(x) \quad (8)$$

$$U_j c_{i\tau}^\dagger(x) U_j = c_{i\tau}^\dagger(x) \quad i \neq j \quad (9)$$

which show that these operators $c_{i\tau}^\dagger(x)$ and $c_{i\tau}(x)$ carry a non-trivial local \mathbb{Z}_2 charge. The precise correspondence between the initial operators $\psi_{ij\alpha\uparrow}^\dagger(x)$ and the cage operators $c_{i\tau}^\dagger(x)$ is as follows:

$$\psi_{ij\alpha\tau}^\dagger(x) = \frac{1}{\sqrt{2}} \left(e^{-i\theta_{ij\alpha}(x)} c_{i\tau}^\dagger(x) + e^{-i\theta_{jia}(x)} c_{j\tau}^\dagger(x) \right) \quad (10)$$

where $\theta_{ij\alpha}(x) = \frac{e}{\hbar} \int_i^x \mathbf{A}_{ij\alpha} \cdot d\mathbf{r}$ is a line integral oriented from node i to node j . The local Hubbard interaction in

cage basis takes the following form:

$$\begin{aligned} \psi_{ij\alpha\uparrow}^\dagger(x)\psi_{ij\alpha\downarrow}^\dagger(x)\psi_{ij\alpha\downarrow}(x)\psi_{ij\alpha\uparrow}(x) &= & (11) \\ c_{i\uparrow}^\dagger(x)c_{i\downarrow}^\dagger(x)c_{i\downarrow}(x)c_{i\uparrow}(x) + c_{j\uparrow}^\dagger(x)c_{j\downarrow}^\dagger(x)c_{j\downarrow}(x)c_{j\uparrow}(x) &+ & [a] \\ c_{i\uparrow}^\dagger(x)c_{j\downarrow}^\dagger(x)c_{j\downarrow}(x)c_{i\uparrow}(x) + c_{j\uparrow}^\dagger(x)c_{i\downarrow}^\dagger(x)c_{i\downarrow}(x)c_{j\uparrow}(x) &+ & [b] \\ c_{i\uparrow}^\dagger(x)c_{j\downarrow}^\dagger(x)c_{i\downarrow}(x)c_{j\uparrow}(x) + c_{j\uparrow}^\dagger(x)c_{i\downarrow}^\dagger(x)c_{j\downarrow}(x)c_{i\uparrow}(x) &+ & [c] \\ c_{i\uparrow}^\dagger(x)c_{i\downarrow}^\dagger(x)c_{j\downarrow}(x)c_{j\uparrow}(x) + c_{j\uparrow}^\dagger(x)c_{j\downarrow}^\dagger(x)c_{i\downarrow}(x)c_{i\uparrow}(x) &+ & [d] \end{aligned}$$

Lines on the right-hand side represent respectively: an intra-cage Hubbard interaction [a], an inter-cage Hubbard interaction [b], a neighbor cage exchange process [c], a pair propagation process [d].

In the case of a one-dimensional chain of loops, these various processes may be visualized directly on the graph shown on Fig. 4.

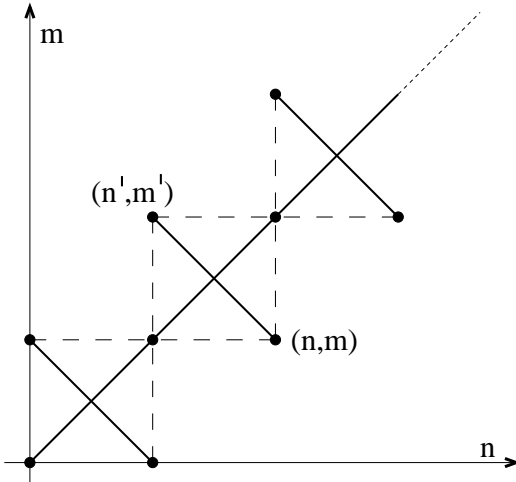


FIG. 4: In the case of Hubbard like interacting electrons, the only possible cage transitions preserving local \mathbb{Z}_2 symmetry can be plotted on the following graph (thin lines), where (n, m) and (n', m') indicate initial and final cage positions, corresponding to a term $c_{n'}^\dagger c_{m'}^\dagger c_m c_n$. Dashed lines refer to possible non zero amplitude transitions, compatible with the local nature of two-electron interaction, but which are forbidden since they violate electron number parity conservation resulting from the local \mathbb{Z}_2 symmetry.

The main feature appearing in this new basis is that the parity of the total electron number in *each* Aharonov-Bohm cage is *separately* conserved. Because an electron in state $c_{i\tau}^\dagger(x)|0\rangle$ carries a non-trivial \mathbb{Z}_2 charge, but a pair $c_{i\uparrow}^\dagger(x)c_{i\downarrow}^\dagger(x)|0\rangle$ belongs to the identity representation of the local \mathbb{Z}_2 group, the previous statement simply shows that the local Hubbard interaction commutes with the local \mathbb{Z}_2 symmetry. In Section III B, we show that any pair potential interaction of the form $V(\mathbf{r}, \mathbf{r}')$ is compatible with the local \mathbb{Z}_2 symmetry provided $V(\mathbf{r}, \mathbf{r}')$ does not change when \mathbf{r} or \mathbf{r}' is replaced by its mirror image with respect to the axis joining its two nearest nodes. In a previous work, a similar statement was reached for a rather special case, namely a chain of rhombi in a tight-

binding description¹¹. The present formulation is much more general.

What are the consequences of this local symmetry on an interacting system? As in^{9,10}, let us first consider a pair of electrons, with the local Hubbard interaction. We have three possible situations. First, the two electrons may be located in two cages i and j which do not share common links, that is i and j are not nearest neighbors. Then they do not “see” each other and remain localized in their respective cages. A second possibility occurs when i and j are distinct but nearest neighbors. As term [c] in Eq. (11) above shows, the two electrons can exchange their cages, but such state remains localized under time evolution. Finally, when $i = j$, term [d] in Eq. (11) indicates that a delocalized two electron state is now possible in spite of the purely localized nature of the single particle spectrum and the repulsive character of the interaction.

Of course, the most interesting question is to consider a system with a finite electronic density. As we have seen, because of the local \mathbb{Z}_2 symmetry, only pairs of electrons can propagate in a \mathbb{Z}_2 network. In particular, the single electron propagator $-i\langle c_{i\tau}(x, t)c_{j\tau}^\dagger(x', t')\rangle$ vanishes when $i \neq j$, since it is not \mathbb{Z}_2 invariant, and it is very difficult to break spontaneously a local symmetry²¹. This shows that the low-energy behavior of an electron fluid on a \mathbb{Z}_2 network is *not* described by the Landau model of a Fermi liquid. As we shall see in section IV below, it corresponds most likely to a new form of incoherent metal. But at this stage, the most natural thing to check is whether a superconducting instability (induced by term [d] in Eq. (11)) occurs or not.

B. Mean-field analysis of superconducting instability

To begin this discussion, let us first consider a larger class of electron-electron interaction. The most general two-body potential interaction respecting the global spin rotation symmetry reads:

$$\begin{aligned} \hat{V} = \sum_{ij, i'j'} \sum_{\alpha\alpha'} \sum_{\tau\tau'} & \int_0^{l_{ij}} dx \int_0^{l'_{i'j'}} dx' V_{ij, i'j'}^{\alpha\alpha'}(x, x') \\ \psi_{ij\alpha\uparrow}^\dagger(x)\psi_{i'j'\alpha'\downarrow}^\dagger(x')\psi_{i'j'\alpha'\downarrow}(x')\psi_{ij\alpha\uparrow}(x) & (12) \end{aligned}$$

In this sum, (ij) and $(i'j')$ are two pairs of nearest-neighbor nodes. As before, α (resp. α') labels one of the two links composing the loop (ij) (resp. $(i'j')$). Let us use the cage basis, defined in Eq. (10) to rewrite this interaction. For this purpose, the first step is to express the local electronic density as:

$$\begin{aligned} \psi_{ij\alpha\uparrow}^\dagger(x)\psi_{ij\alpha\downarrow}(x) &= \frac{1}{2}(c_{i\tau}^\dagger(x)c_{i\tau}(x) + c_{j\tau}^\dagger(x)c_{j\tau}(x)) \\ &+ \frac{1}{2}(e^{-i\theta_{ij\alpha}}c_{i\tau}^\dagger(x)c_{j\tau}(x) + e^{-i\theta_{ji\alpha}}c_{j\tau}^\dagger(x)c_{i\tau}(x)) \end{aligned}$$

Because the flux through each elementary loop is half a flux quantum, $e^{-i\theta_{ij\alpha}} = -e^{-i\theta_{ij\bar{\alpha}}}$. The interaction (12) preserves the local \mathbb{Z}_2 symmetry if and only if the following conditions are satisfied:

$$V_{ij,i'j'}^{\alpha\alpha'}(x, x') = V_{ij,i'j'}^{\bar{\alpha}\bar{\alpha}'}(x, x') = V_{ij,i'j'}^{\alpha\bar{\alpha}'}(x, x') \quad (13)$$

provided the pairs (ij) and $(i'j')$ are distinct, and:

$$V_{ij,ij}^{\alpha\alpha'}(x, x') = V_{ij,ij}^{\bar{\alpha}\bar{\alpha}'}(x, x') \quad (14)$$

The first condition implies that

$$\sum_{\alpha} e^{-i\theta_{ij\alpha}} V_{ij,i'j'}^{\alpha\alpha'}(x, x') = 0$$

when (ij) and $(i'j')$ are distinct, and the second condition that

$$\sum_{\alpha, \alpha'} e^{-i\theta_{ij\alpha}} V_{ij,ij}^{\alpha\alpha'}(x, x') = 0$$

Therefore, all the terms which do not preserve the parity of the total electron number in each cage are eliminated. When both conditions (13), (14) on the interaction potential are satisfied, the interaction term (12) now becomes:

$$\begin{aligned} \hat{V} = & \sum_{ij,i'j'} \sum_{\alpha\alpha'} \sum_{\tau\tau'} \int_0^{l_{ij}} dx \int_0^{l'_{ij}} dx' V_{ij,i'j'}^{\alpha\alpha'}(x, x') \\ & \times \left\{ : \left[c_{i\tau}^{\dagger}(x) c_{i\tau}(x) + c_{j\tau}^{\dagger}(x) c_{j\tau}(x) \right] \left[c_{i'\tau'}^{\dagger}(x') c_{i'\tau'}(x') + c_{j'\tau'}^{\dagger}(x') c_{j'\tau'}(x') \right] : \right. \\ & \left. + \delta_{ij,i'j'} : \left[e^{-i\theta_{ij\alpha}} c_{i\tau}^{\dagger}(x) c_{j\tau}(x) + e^{-i\theta_{j\tau\alpha}} c_{j\tau}^{\dagger}(x) c_{i\tau}(x) \right] \left[e^{-i\theta_{ij\alpha'}} c_{i\tau}^{\dagger}(x') c_{j\tau}(x) + e^{-i\theta_{j\tau\alpha'}} c_{j\tau}^{\dagger}(x) c_{i\tau}(x) \right] : \right\} \end{aligned} \quad (15)$$

We have used the standard notation : \mathcal{O} : for the normal ordering of the operator \mathcal{O} .

Let us now consider the possibility of a superconducting instability. In a variational approach, we would use a Hartree-Fock-Bogoliubov trial state. In the presence of pairing, the average kinetic energy increases, so it would have to be compensated by a lowering in the average interaction energy. As usual, this quantity involves averages of the form $\langle c^{\dagger} c \rangle \langle c^{\dagger} c \rangle$ and of the form $\langle c^{\dagger} c^{\dagger} \rangle \langle c c \rangle$. In the spirit of a mean field theory, we shall keep only the latter terms. Once again we also argue that the local \mathbb{Z}_2 symmetry is not broken, even in the hypothetical superconducting state. Physically, this is reasonable since the size of the Aharonov-Bohm cages being finite, there is a finite gap between the \mathbb{Z}_2 sector with $\epsilon_i = 1$ and the sector with $\epsilon_i = -1$. As discussed below, this gap can be as large as a few Kelvin degrees for a GaAs \mathbb{Z}_2 network. With an unbroken \mathbb{Z}_2 symmetry, the superconducting order parameter $\langle c_{i\tau}^{\dagger}(x) c_{j\tau}^{\dagger}(x') \rangle$ vanishes if $i \neq j$.

Let us first consider a singlet pairing. This leads to:

$$\begin{aligned} \langle c_{i\uparrow}^{\dagger}(x) c_{i\uparrow}^{\dagger}(x') \rangle &= \langle c_{i\downarrow}^{\dagger}(x) c_{i\downarrow}^{\dagger}(x') \rangle = 0 \\ \langle c_{i\uparrow}^{\dagger}(x) c_{i\downarrow}^{\dagger}(x') \rangle &= -\langle c_{i\downarrow}^{\dagger}(x) c_{i\uparrow}^{\dagger}(x') \rangle = \Delta_i(x, x') \end{aligned}$$

In this case, the local contribution of Cooper pairing to the trial potential energy is:

$$V_{ij,i'j'}^{\alpha\alpha'}(x, x') |e^{-\frac{i}{2}\theta_{ij\alpha}} \Delta_i(x, x') + e^{-\frac{i}{2}\theta_{j\tau\alpha}} \Delta_j(x, x')|^2 \quad (16)$$

In the case of triplet pairing, we have a complex vector $\Delta_j(x, x')$ defined by:

$$\begin{aligned} \Delta_j^x(x, x') &= \frac{1}{\sqrt{2}} \langle -c_{j\uparrow}^{\dagger}(x) c_{j\uparrow}^{\dagger}(x') + c_{j\downarrow}^{\dagger}(x) c_{j\downarrow}^{\dagger}(x') \rangle \\ \Delta_j^y(x, x') &= \frac{i}{\sqrt{2}} \langle c_{j\uparrow}^{\dagger}(x) c_{j\uparrow}^{\dagger}(x') + c_{j\downarrow}^{\dagger}(x) c_{j\downarrow}^{\dagger}(x') \rangle \\ \Delta_j^z(x, x') &= \frac{1}{\sqrt{2}} \langle c_{j\uparrow}^{\dagger}(x) c_{j\downarrow}^{\dagger}(x') + c_{j\downarrow}^{\dagger}(x) c_{j\uparrow}^{\dagger}(x') \rangle \end{aligned}$$

For triplet pairing, the orbital angular momentum of a Cooper pair is odd, so $\Delta_j(x, x') = -\Delta_j(x', x)$. It is simple to check that the above expression (16) still applies up to replacing the complex scalar $\Delta_j(x, x')$ by the complex vector $\Delta_j(x, x')$.

To conclude, we show that the part of the trial energy which is directly sensitive to a \mathbb{Z}_2 invariant Cooper pairing amplitude is positive for a positive interaction potential compatible with the local \mathbb{Z}_2 symmetry. So, at least in a mean-field picture, a superconducting instability cannot occur. This statement was not a priori obvious, given the existence of delocalized states for the two-particle problem, where both particles are located in the same cage at any time, even with a repulsive interaction.

C. Discussion for networks in semiconductor heterostructures

For applications to real systems, it is important to present some order of magnitude estimates. For wires etched on a 2D electron gas at a GaAs/GaAlAs interface, with a typical carrier density of $3 \cdot 10^{11} \text{ cm}^{-2}$ and a transverse width $w = 100 \text{ nm}$, the number of transverse conduction channels $N = k_{\text{F}}w/\pi$ is around 4. For a regular network of single channel wires, we have investigated interaction effects on the low-energy scattering matrix at the nodes²². The renormalization of the transmission coefficient $T(\Lambda)$ as a function of a typical energy scale Λ is given by:

$$T(\Lambda) = \frac{T_0(\Lambda/\Lambda_0)^{2\alpha}}{R_0 + T_0(\Lambda/\Lambda_0)^{2\alpha}}, \quad (R_0 + T_0 = 1) \quad (17)$$

where $\alpha = \tilde{U}(k \rightarrow 0)/(hv_{\text{F}})$ is proportional to the Fourier transform of the interaction potential in the long wavelength limit. This result corresponds to nodes having a complete symmetry under any permutation of the incident wires. Note that it has the same form as for a single elastic scatterer in a Luttinger liquid^{23,24}, or a single crossing connecting several semi-infinite Luttinger liquids²⁵. For a single wire of width w and length L , $\tilde{U}(k \rightarrow 0) \simeq \frac{e^2}{4\pi\epsilon_0\epsilon_r} \ln(2L/w)$. Choosing typical values as $m^* = 0.067 \text{ m}_e$ and $\epsilon_r = 12.9$ for GaAs, $L = 2 \mu\text{m}$ and $w = 100 \text{ nm}$, we obtain $\alpha = 0.4$ which is a rather large value. This shows that the Coulomb energy is nearly as large as the kinetic energy of conduction electrons.

As usual for 1D electron systems with repulsive interactions, the leading instability occurs because of the divergence of the static charge and spin susceptibilities at the wave-vector $q = 2k_{\text{F}}$ and favors the formation of a spin-density wave. A derivation of this mean-field transition on a \mathbb{Z}_2 network is sketched in Appendix A. But with $\alpha = 0.4$, the critical temperature for the onset of this mean-field instability is not much smaller than the Fermi energy (see for instance Eq. (A1)), which shows that the system is still in a one-dimensional regime. Indeed, the cross-over from one to two dimensions takes place when the 1D thermal length $L_{\text{T}} = hv_{\text{F}}/k_{\text{B}}T$ becomes comparable to the distance L between nearest-neighbor nodes. In other words, the corresponding energy scale $k_{\text{B}}T$ should be as low as the energy level splittings inside Aharonov-Bohm cages, that is of the order of hv_{F}/L . Since $\lambda_{\text{F}} = 50 \text{ nm}$ ($L/\lambda_{\text{F}} = 40$), the cross-over to 2D behavior appears at an energy scale one order of magnitude smaller than the mean-field Peierls instability scale. In practice however, because of the small effective mass in GaAs, the low energy scale hv_{F}/L can be of the order of a few Kelvin degrees. This scale sets also the order of magnitude of the \mathbb{Z}_2 gap already mentioned.

It is well-known that in a purely 1D system, fluctuations in the Peierls and in the Cooper channels have a tendency to neutralize each other, and the result is in general some kind of Luttinger liquid²⁶. As mean-field

analysis fails to predict such a behavior, we should therefore revisit the result of the previous section using an approach which is able to treat both Peierls and Cooper channels on an equal footing. This is exactly what the renormalization group (RG) is able to provide, at least in the weak interaction limit. To be completely honest, it is not at all clear that a perturbative RG can give reliable quantitative estimates when α is as large as 0.4. But for the sake of establishing the presence or the absence of an instability, we expect it to produce a valid qualitative picture, specially in the case, as we shall see below, where it predicts an instability to a gapped state already for small coupling. It might happen, as in some Hubbard models with extended internal symmetries²⁸, that some features of the gapped phase are modified when the coupling becomes large compared to the electronic bandwidth. But in this example, the gap never closes when the system evolves from weak to strong coupling.

IV. RENORMALIZATION GROUP ANALYSIS

A. Low-energy model

A complete RG analysis for our original system would be very complicated, because of the absence of translation invariance inside Aharonov-Bohm cages. In particular, network nodes induce Friedel density oscillations in the electron fluid, which renormalize the associated single electron scattering matrices in the presence of interactions. This mechanism is precisely at the origin of the scaling shown in Eq. (17)^{22,24,25}. Physically, this interaction effect shows that wires have a tendency to become disconnected at low energies, which stops below the cross-over into the 2D regime. As shown previously²², an electronic wire network becomes an insulator for commensurate filling factors, or simply highly resistive, with a weakly dispersive band crossing the Fermi level for generic filling factors. However, for a system with local \mathbb{Z}_2 symmetry, this renormalization mostly modifies the internal dynamics inside a given Aharonov-Bohm cage, and not the general structure of the electron-electron interaction as it appears in Eq. (11). At this point, we shall now assume that details of this internal dynamics inside Aharonov-Bohm cages do not play much role in the analysis of interaction effects at low energy, provided the local \mathbb{Z}_2 symmetry manifested in Eq. (11) is still respected. The validity of this assumption will be examined in more detail at the end of this section, once the results of the RG treatment are available.

This leads us to consider the following model, where each Aharonov-Bohm cage is replaced by an infinite 1D Luttinger liquid, described by the electronic fields $c_{i\tau}^{\dagger}(x)$, $c_{i\tau}(x)$, i being a cage label and τ the spin projection. The internal energy levels of this collection of modified Aharonov-Bohm cages is naturally described by the following kinetic Hamiltonian:

$$H_0 = \int_{-\infty}^{\infty} dx \sum_j \sum_{\tau} : \left[c_{R,j,\tau}^{\dagger}(x) \frac{1}{i} \frac{d}{dx} c_{R,j,\tau}(x) - c_{L,j,\tau}^{\dagger}(x) \frac{1}{i} \frac{d}{dx} c_{L,j,\tau}(x) \right] : \quad (18)$$

where $h\nu_F$ has been set equal to unity. As usual, right and left moving fields have been introduced, labelled by R and L respectively, so that $c_{i\tau}^{\dagger}(x) = c_{R,i,\tau}^{\dagger}(x) + c_{L,i,\tau}^{\dagger}(x)$. Note that replacing finite Aharonov-Bohm cages by infinite ones is only valid in the 1D regime, when we can neglect the discrete nature of the single particle spectrum. The physical motivation for doing this is that as discussed in the previous section, the typical interaction scale is larger than the \mathbb{Z}_2 gap in present experiments. On the other hand, the perturbative RG used here requires

small interactions in comparison to the single electron bandwidth. Because of the large value of L/λ_F , these two requirements are mutually compatible.

Two nearby cages i and j are coupled by a two-body interaction subjected to the following constraints: it has to preserve the local \mathbb{Z}_2 symmetry or equivalently, to conserve the parity of the total number of electrons in each cage, and to simplify the treatment, to preserve also the translational symmetry within cages. Both requirements are satisfied by the following Hubbard-like interaction:

$$H_{\text{int}} = U \int_{-\infty}^{\infty} dx \sum_{i,j} : \left[c_{i\uparrow}^{\dagger}(x) c_{i\downarrow}^{\dagger}(x) c_{i\downarrow}(x) c_{i\uparrow}(x) + c_{j\uparrow}^{\dagger}(x) c_{j\downarrow}^{\dagger}(x) c_{j\downarrow}(x) c_{j\uparrow}(x) + c_{i\uparrow}^{\dagger}(x) c_{i\downarrow}^{\dagger}(x) c_{j\downarrow}(x) c_{i\uparrow}(x) + c_{j\uparrow}^{\dagger}(x) c_{i\downarrow}^{\dagger}(x) c_{j\downarrow}(x) c_{j\uparrow}(x) + c_{i\uparrow}^{\dagger}(x) c_{j\downarrow}^{\dagger}(x) c_{i\downarrow}(x) c_{j\uparrow}(x) + c_{j\uparrow}^{\dagger}(x) c_{i\downarrow}^{\dagger}(x) c_{j\downarrow}(x) c_{i\uparrow}(x) + c_{i\uparrow}^{\dagger}(x) c_{i\downarrow}^{\dagger}(x) c_{j\downarrow}(x) c_{j\uparrow}(x) + c_{j\uparrow}^{\dagger}(x) c_{j\downarrow}^{\dagger}(x) c_{i\downarrow}(x) c_{i\uparrow}(x) \right] :$$

Using the decomposition $c_{i\tau}^{\dagger}(x) = c_{R,i,\tau}^{\dagger}(x) + c_{L,i,\tau}^{\dagger}(x)$ generates many terms, among which we shall neglect two subsets. The first subset contains all the purely forward scattering processes on a given side of the Fermi-surface, i.e. of the form $c_R^{\dagger}c_R^{\dagger}c_Rc_R$ or $c_L^{\dagger}c_L^{\dagger}c_Lc_L$. In perturbation theory, they do not give singular terms in the low-energy limit, so we shall ignore them. The second subset contains all Umklapp terms, of the form $c_R^{\dagger}c_R^{\dagger}c_Lc_R$ (resp. $c_R^{\dagger}c_R^{\dagger}c_Lc_L$) which are relevant only for a filled (resp. half-filled) single electron band. The most interesting terms are of the type $c_R^{\dagger}c_L^{\dagger}c_Lc_R$ which induce logarithmic divergences to the dressed two-particle interaction in the

low energy limit. These terms are adequately treated by the renormalization group. Introducing now generalized charge and spin densities defined as:

$$\rho_{R(L),n,n'}(x) = \sum_{\tau,\tau'} c_{R(L),n,\tau}^{\dagger}(x) \delta_{\tau,\tau'} c_{R(L),n',\tau'}(x), \quad (19)$$

$$\mathbf{S}_{R(L),n,n'}(x) = \sum_{\tau,\tau'} c_{R(L),n,\tau}^{\dagger}(x) \boldsymbol{\sigma}_{\tau,\tau'} c_{R(L),n',\tau'}(x), \quad (20)$$

where $\boldsymbol{\sigma} = (\sigma^x, \sigma^y, \sigma^z)$ are the usual Pauli matrices, we may finally write the interaction term in the form:

$$H_{\text{int}} = U \int_{-\infty}^{\infty} dx \sum_n : \left[2\rho_{R,n,n}(x) \rho_{L,n,n}(x) - 2\mathbf{S}_{R,n,n} \mathbf{S}_{L,n,n} \right. \\ \left. + \rho_{R,n,n}(x) \rho_{L,n+1,n+1}(x) - \mathbf{S}_{R,n,n} \mathbf{S}_{L,n+1,n+1} + \rho_{R,n+1,n+1}(x) \rho_{L,n,n}(x) - \mathbf{S}_{R,n+1,n+1} \mathbf{S}_{L,n,n} \right. \\ \left. + \rho_{R,n+1,n}(x) \rho_{L,n,n+1}(x) - \mathbf{S}_{R,n+1,n} \mathbf{S}_{L,n,n+1} + \rho_{R,n,n+1}(x) \rho_{L,n+1,n}(x) - \mathbf{S}_{R,n,n+1} \mathbf{S}_{L,n+1,n} \right. \\ \left. + \rho_{R,n+1,n}(x) \rho_{L,n+1,n}(x) - \mathbf{S}_{R,n+1,n} \mathbf{S}_{L,n+1,n} + \rho_{R,n,n+1}(x) \rho_{L,n,n+1}(x) - \mathbf{S}_{R,n,n+1} \mathbf{S}_{L,n,n+1} \right] : . \quad (21)$$

Here, we have chosen a particular 1D geometry, namely a chain of loops. Although the RG approach could be ap-

plied to any regular lattice of Luttinger liquid-like cages, we shall from now on focus on this example. The re-

sults we shall present shortly suggest that the large scale lattice geometry does not affect much the physical properties of such a system.

B. Renormalization group equations

We shall now briefly derive one-loop RG equations. We refer the reader to Ref. 27 and references therein for general details about the RG technique. Here we focus on what happens in the space of cage positions, since this is

what makes the originality of our work. The microscopic Hamiltonian (18-21) serves as the high energy initial condition of RG flows. The kinetic part of the Hamiltonian is unrenormalized at one-loop order, while the interaction part flows. During the renormalization process, the interactions will develop a non-trivial dependence in the cage positions. The local \mathbb{Z}_2 -symmetry as well as the translational symmetry of the initial Hamiltonian (18-21) will remain symmetries of the renormalized Hamiltonian. As a consequence, the flowing Hamiltonian is constrained to be of the following form

$$H_0(\Lambda) = \int_{-\Lambda}^{\Lambda} \frac{dk}{2\pi} \sum_n \sum_{\tau} : \left[k c_{R,n,\tau}^{\dagger}(k) c_{R,n,\tau}(k) - k c_{L,n,\tau}^{\dagger}(k) c_{L,n,\tau}(k) \right] : \quad (22)$$

$$H_{\text{int}}(\Lambda) = \int_{-\Lambda}^{\Lambda} \frac{dq}{2\pi} \sum_n : \left\{ \sum_{\gamma \neq 0} \left[A_{\gamma}^c(\Lambda) \rho_{R,n,n}(q) \rho_{L,n+\gamma,n+\gamma}(-q) + A_{\gamma}^s(\Lambda) \mathbf{S}_{R,n,n}(q) \mathbf{S}_{L,n+\gamma,n+\gamma}(-q) \right. \right. \\ \left. \left. + B_{\gamma}^c(\Lambda) \rho_{R,n+\gamma,n}(q) \rho_{L,n,n+\gamma}(-q) + B_{\gamma}^s(\Lambda) \mathbf{S}_{R,n+\gamma,n}(q) \mathbf{S}_{L,n,n+\gamma}(-q) \right. \right. \\ \left. \left. + C_{\gamma}^c(\Lambda) \rho_{R,n+\gamma,n}(q) \rho_{L,n+\gamma,n}(-q) + C_{\gamma}^s(\Lambda) \mathbf{S}_{R,n+\gamma,n}(q) \mathbf{S}_{L,n+\gamma,n}(-q) \right] \right. \\ \left. + D^c(\Lambda) \rho_{R,n,n}(q) \rho_{L,n,n}(-q) + D^s(\Lambda) \mathbf{S}_{R,n,n}(q) \mathbf{S}_{L,n,n}(-q) \right\} : . \quad (23)$$

Note that the hermiticity of the Hamiltonian implies that $C_{-\gamma}^{c(s)} = C_{\gamma}^{c(s)}$, and the Right/Left symmetry gives $A_{-\gamma}^{c(s)} = A_{\gamma}^{c(s)}$ and $B_{-\gamma}^{c(s)} = B_{\gamma}^{c(s)}$. The action of the four types of locally \mathbb{Z}_2 -symmetric couplings A_{γ} , B_{γ} , C_{γ} and D (forgetting about their charge/spin nature) are represented in Fig. 5.

In Eqs. (22-23) we used the Fourier transform of the field operators which is defined by

$$c_{R(L),n,\tau}(k) = \int_{-\infty}^{\infty} dx \exp(-ikx) c_{R(L),n,\tau}(x). \quad (24)$$

The Fourier transform of the generalized charge density, for example, is given by

$$\rho_{R(L),n,n'}(q) = \int_{-\infty}^{\infty} dx \exp(iqx) \rho_{R(L),n,n'}(x) \quad (25)$$

$$= \int_{-\Lambda}^{\Lambda} \frac{dk}{2\pi} \sum_{\tau} c_{R(L),n,\tau}^{\dagger}(k+q) c_{R(L),n',\tau}(k),$$

All momenta have been restricted to be smaller in absolute value than the cut-off Λ , in order to regularize

ultra-violet divergences. Note that the Fermi momentum has been set to zero, which is allowed since we do not consider Umklapp processes. We have not denoted any momentum dependence of the interactions, because in the RG treatment, all momenta are taken at the Fermi surface.

The high-energy Hamiltonian is defined at scale Λ_0 , and the initial conditions of the RG flow, at this scale, are found from (21) and read

$$\begin{aligned} A_{\gamma}^c(\Lambda_0) &= B_{\gamma}^c(\Lambda_0) = C_{\gamma}^c(\Lambda_0) = U(\delta_{\gamma,1} + \delta_{\gamma,-1}) \\ A_{\gamma}^s(\Lambda_0) &= B_{\gamma}^s(\Lambda_0) = C_{\gamma}^s(\Lambda_0) = -U(\delta_{\gamma,1} + \delta_{\gamma,-1}) \\ D^c(\Lambda_0) &= 2U \\ D^s(\Lambda_0) &= -2U \end{aligned} \quad (26)$$

The interactions are renormalized both by particle-hole and particle-particle contributions. Written with the dimensionless scale $l = \ln(\Lambda_0/\Lambda)$, the RG equations are

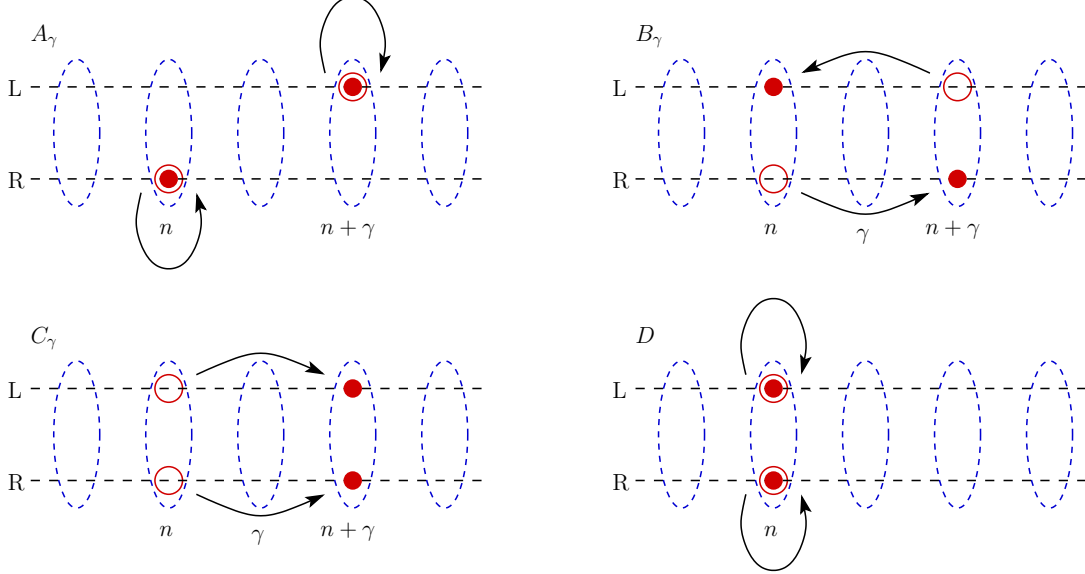


FIG. 5: Schematic representation of the four interactions compatible with the local \mathbb{Z}_2 -symmetry, given in Eq. (23). Each dashed ellipse represents a cage. An empty (full) circle represents a destruction (creation) operator. Coupling A is an inter-cage interaction, coupling B a cage exchange, coupling C a pair hopping, and coupling D an intra-cage interaction.

$$\partial_l A_\gamma^{c(s)} = [A_\gamma * A_\gamma + C_\gamma * C_{-\gamma}]_{ph}^{c(s)} + [A_\gamma * A_\gamma + B_\gamma * B_{-\gamma}]_{pp}^{c(s)}, \quad (27)$$

$$\partial_l B_\gamma^{c(s)} = [2D * B_\gamma + \sum_{\beta \neq 0, \gamma} B_\beta * B_{\gamma-\beta}]_{ph}^{c(s)} + [B_\gamma * (A_\gamma + A_{-\gamma})]_{pp}^{c(s)}, \quad (28)$$

$$\partial_l C_\gamma^{c(s)} = [C_\gamma * (A_\gamma + A_{-\gamma})]_{ph}^{c(s)} + [2D * C_\gamma + \sum_{\beta \neq 0, \gamma} C_\beta * C_{\gamma-\beta}]_{pp}^{c(s)}, \quad (29)$$

$$\partial_l D^{c(s)} = [D * D + \sum_{\beta \neq 0} B_\beta * B_{-\beta}]_{ph}^{c(s)} + [D * D + \sum_{\beta \neq 0} C_\beta * C_{-\beta}]_{pp}^{c(s)}. \quad (30)$$

In these flow equations, we have denoted

$$[G_1 * G_2]_{ph}^c = \frac{1}{2\pi} (G_1^c G_2^c + 3G_1^s G_2^s), \quad (31)$$

$$[G_1 * G_2]_{ph}^s = \frac{1}{2\pi} (G_1^s G_2^c + G_1^c G_2^s + 2G_1^s G_2^s), \quad (32)$$

for the particle-hole channel, and

$$[G_1 * G_2]_{pp}^c = -\frac{1}{2\pi} (G_1^c G_2^c + 3G_1^s G_2^s), \quad (33)$$

$$[G_1 * G_2]_{pp}^s = -\frac{1}{2\pi} (G_1^s G_2^c + G_1^c G_2^s - 2G_1^s G_2^s), \quad (34)$$

for the particle-particle channel. The RG flow equations can be simplified further, but we shall leave them in the form (27-30) because it clearly shows the origin of all one-loop contributions. As an illustration, we show in Fig. 6 the bubbles renormalizing the pair hopping term C_γ .

C. Numerical solution of the Renormalization Group equations

1. Strong coupling Hamiltonian

The flow equations (27-30) cannot be solved analytically, but one can integrate them numerically with standard numerical routines such as Runge-Kutta of order 4. One nice feature of the local \mathbb{Z}_2 -symmetry is that it constrains interactions in such a way that they can depend on at most one cage index. Thus the number of equations that have to be solved only grows linearly with the total number of cages N , allowing to consider large system sizes.

With the initial conditions (26), we found that the system goes to strong coupling. The flow diverges at a critical RG scale l_c , indicating a phase transition at a critical

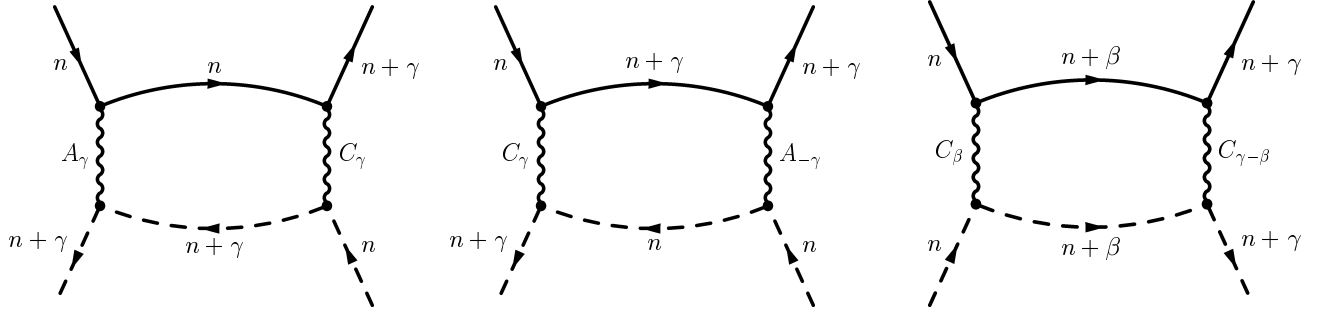


FIG. 6: Graphs renormalizing the pair hopping term C_γ . The left and middle graphs are particle-hole bubbles, and the right one is a particle-particle bubble. For the latter, β is summed over, and when $\beta = 0$ or γ , the quantity C_0 that appears should be understood as D , so as to yield Eq. (29).

temperature of order of magnitude $T_c = \Lambda_0 \exp(-l_c)$. Apart from finite-size corrections, the numerical solution of the flow reaches the following fixed direction

$$A_\gamma^c = A_\gamma^s = 0, \quad (35)$$

$$B_\gamma^c = D^c = -3B_\gamma^s = -3D^s > 0, \quad (36)$$

$$C_\gamma^c = C_\gamma^s = 0, \quad (37)$$

for any value of γ . The corresponding effective interaction Hamiltonian can be written (going back to real space and setting the strength of the interaction to a value g)

$$H_{\text{int}}^{\text{eff}} = g \int_{-\infty}^{\infty} dx \sum_{n,\gamma} : [3\rho_{R,n+\gamma,n}(x)\rho_{L,n,n+\gamma}(x) - S_{R,n+\gamma,n}(x)S_{L,n,n+\gamma}(x)] : \quad (38)$$

This Hamiltonian has an $SU(N)$ symmetry in the cage indices, and it corresponds to a particle-hole pairing in the triplet channel. Consequently the system undergoes a phase transition to a spin-density wave state, as was predicted by our mean-field analysis (see appendix A). This is more transparent on the equivalent form of (38):

$$H_{\text{int}}^{\text{eff}} = -2g \int_{-\infty}^{\infty} dx \sum_{m,n} \sum_{\mu\mu'} \sum_{\nu\nu'} : (c_{R,m,\mu}^\dagger(x) \sigma_{\mu,\mu'} c_{L,m,\mu'}(x)) (c_{L,n,\nu}^\dagger(x) \sigma_{\nu,\nu'} c_{R,n,\nu'}(x)) : \quad (39)$$

since it is bilinear in the $2k_F$ Fourier component of the local spin density. A more detailed analysis of this phase, including a discussion of its collective modes can be found in Ref. 27.

The RG calculation however gives a much smaller value of the critical temperature than the mean-field calculation. We have computed the critical temperature given by the full flow equations (27-30), as well as for the RPA approximation of these, which consists in neglecting all particle-particle contributions. We found the following numerical result

$$l_c(\text{RG}) \simeq \frac{1.33}{U} \quad \text{and} \quad l_c(\text{RPA}) \simeq \frac{0.64}{U}. \quad (40)$$

For an initial interaction $U = 0.1$, this gives a ratio $T_c(\text{RG})/T_c(\text{RPA}) \simeq 10^{-3}$, which is very small. The RPA thus overestimates the critical temperature by three orders of magnitude for $U = 0.1$. For the typical value $\alpha = 0.4$ ($U = 2\pi\alpha$) estimated in GaAs networks, this reduction effect is not as dramatic, since here we obtain: $T_c(\text{RG})/T_c(\text{RPA}) \simeq 0.76$. This gives further support to replacing finite Aharonov-Bohm cages by infinite ones in our simplified model, since the energy scale which emerges from the RG treatment is still in the 1D regime, for a typical choice of parameters such as $L/\lambda_F = 40$.

2. Intermediate energy regime

Another feature of the RPA is that the pair hopping terms $C^{c(s)}$ remain nearest neighbor all along the flow, as can be inferred from Eq. (29), when neglecting the particle-particle contribution. This is obviously not the case any more for the full RG equations. As the pair hopping terms are the only processes that can lead to a conducting behavior, it is natural to study what happens to them during the flow, before they get completely suppressed by the spin-density wave.

We found numerically that, except at the very beginning of the flow, the pair hopping terms are very well fitted by the following law

$$C_\gamma^{c(s)}(l) = (-1)^\gamma \Gamma^{c(s)}(l) \exp[-\gamma/\xi^{c(s)}(l)]. \quad (41)$$

This shows the incoherent nature of these pair hopping processes. As an illustration, Fig. 7 shows $\ln |C_\gamma^c(l=1)|$ as a function of γ , for $N = 128$ cages and interaction strength $U = 0.1$. We have performed such fits for many values of l so as to extract the scale dependence of the quantities $\Gamma^{c(s)}(l)$ and $\xi^{c(s)}(l)$ defined in Eq. (7). The results for the charge and spin couplings are nearly identical, so that we only show the behavior of the charge quantities, see Figs. 8 and 9. From Fig. 8, it is clear that the pair hopping is suppressed during the flow, but there is an intermediate energy regime ($2 \lesssim l \lesssim 12$) where the decrease rate of the pair hopping is not too large. Furthermore, we see in Fig. 9 that the typical range of

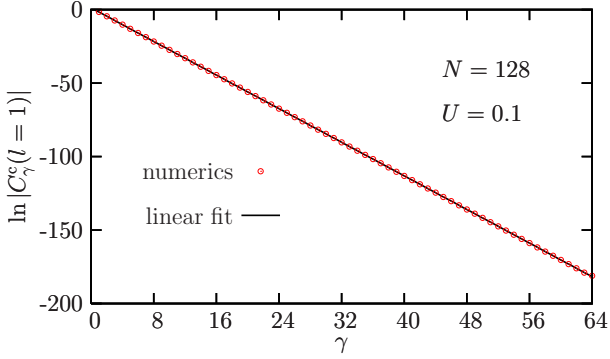


FIG. 7: The numerical results of $\ln |C_\gamma^c(l=1)|$ as a function of γ , for $N = 128$ cages and initial interaction $U = 0.1$, are perfectly fitted by a straight line.

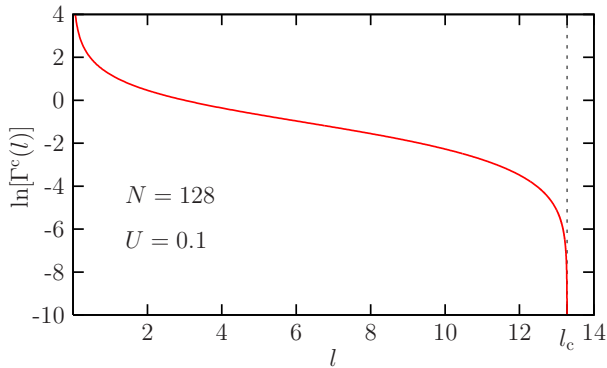


FIG. 8: Evolution of the strength of the interaction $C_\gamma^c(l)$ as a function of the RG scale l , for $N = 128$ cages and initial interaction $U = 0.1$. The flow stops at the critical scale l_c denoted by a dashed line.

the pair hopping increases during the flow, but it does not exceed one lattice spacing. The pair hopping thus remains local, contrarily to the cage exchange terms B_γ which become of infinite range during the flow, as was explained in the previous subsection.

D. Validity of the simplified model

An important question arises: when can the Friedel density oscillations be ignored? In a real system, two physical processes are in competition: the wire disconnection at network junctions due to the S -matrix renormalization, and the SDW instability discussed earlier. In order to estimate the typical energy scale of wire disconnection, we use Eq. (17) and take the point where both terms in the denominator are of the same order of magnitude.

$$k_B T_c(S) \simeq E_F \left(\frac{R_0}{T_0} \right)^{1/2\alpha} \quad (42)$$

The simplified model discussed in this section gives a faithful description of the initial \mathbb{Z}_2 network only if the

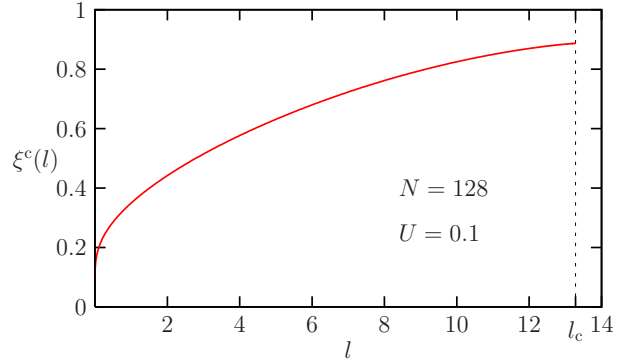


FIG. 9: Evolution of the range of the interaction $C_\gamma^c(l)$ as a function of the RG scale l , for $N = 128$ cages and interaction strength $U = 0.1$. The flow stops at the critical scale l_c denoted by a dashed line.

typical energy scale for the SDW instability is larger than $T_c(S)$. From (40), we have:

$$k_B T_c(\text{RG}) \simeq E_F \exp \left(-\frac{1.33}{U} \right) \quad (43)$$

This gives a rather precise criterion, namely:

$$\frac{R_0}{T_0} < \exp \left(-\frac{1.33}{\pi} \right) \simeq 0.655 \quad (44)$$

Note that because of the one loop RG approximation used for both mechanisms (i.e scattering on Friedel oscillations, and SDW instability), this criterion is independent of the interaction strength, provided it is small compared to the electronic Fermi energy. We may say that it is of a purely geometric nature, since it mostly depends on the amount of electronic backscattering induced by the network nodes. For an illustration, let us consider the two types of node geometries depicted on Fig. 3. For single mode wires, we have found that the lowest values of the ratio R_0/T_0 for perfectly symmetric X or Y junctions are equal respectively to 1 and $1/4$. So changing the junction type from X (Fig. 3 a)) to Y (Fig. 3 b)) could affect deeply the nature of the low-energy state.

In the case of a single 1D quantum wire, the RG approach gives a vanishing transition temperature and the spin density wave is replaced by a Luttinger liquid fixed point at low energy. For \mathbb{Z}_2 networks in the regime where $T_c(\text{RG}) > T_c(S)$, inter-cage interaction processes destroy this Luttinger liquid, and because of the flow to strong coupling, most elementary excitations acquire a gap of the order $T_c(\text{RG})$. In the other regime, ($T_c(\text{RG}) < T_c(S)$), our simplified model discarding Friedel oscillations cannot capture the low energy physics below $T_c(S)$. Below this scale, the network “breaks” into independent disconnected links, which are expected to behave as independent finite segments of Luttinger liquids.

How could we distinguish between these two situations in real experiments? It may not be very easy at a qualitative level, just looking at transport measurements. Re-

sistivity is expected to rise sharply below the largest temperature scale between $T_c(\text{RG})$ and $T_c(\text{S})$, but for very different reasons in each case. If $T_c(\text{RG}) > T_c(\text{S})$, the single electron spectrum is gapped, and charge transport is provided only via a single charge collective mode, which is likely to be quite sensitive to pinning by random impurities. If $T_c(\text{RG}) < T_c(\text{S})$, the disconnection of the network into independent segments clearly induces a very high resistivity. The difference between the two situations could be evidenced by *non-linear* dc-transport. Indeed, in the former situation, a pinned spin-density wave can be depinned by a large enough electric field, and should lead to a large non-linear dc conductivity above a finite threshold value for the driving field. In the later case, possible non-linear effects on the disconnection mechanism have not been investigated to our knowledge. But it seems unlikely that they would yield a sharp threshold as in the case of collective depinning.

The above discussion shows that it would be crucial to estimate the ratio R_0/T_0 for a given sample. In present experiments, although the number of channels N_{ch} is low (about five), it is not exactly one. So we have a $Z \times N_{\text{ch}}$ conduction matrix at each node connected to Z nearest neighbors. This clearly calls for an extension of the theory to the case of multichannel wires, which goes beyond the scope of the present work. But even for a strictly single channel network, a direct experimental determination of R_0/T_0 may not be straightforward. In a dc transport measurement of an *ideal* system, the Landauer approach shows that the resistivity is dominated by the contacts between the network and the outer current leads. As shown in²², R_0/T_0 controls the dispersion of the mini energy bands associated to the lattice superstructure. If R_0/T_0 is small, these bands are weakly dispersive, and the effect of static random impurities, always present in a real system, is stronger than for a large value of R_0/T_0 . But in general, we do not have an independent measurement of the disorder strength. So at this stage, the main prediction is that some \mathbb{Z}_2 networks should develop a SDW instability and some others break into independent disconnected segments at low energy. Although the mathematical criterion (44) is quite precise and simple, it may be difficult *in practise* to decide if a given sample will fall in one or the other class without actually doing the experiment.

V. CONCLUSION

In this paper, we have studied a class of networks (\mathbb{Z}_2 networks) for which all single electron energy eigenstates are localized in Aharonov-Bohm cages when an external magnetic field corresponding to half a flux quantum per loop is applied. The particularity of these networks (in comparison to other geometries showing Aharonov-Bohm cages such as the dice lattice), is the presence of a large group of local \mathbb{Z}_2 symmetries, which correspond to reversing the electronic current in all the loops adja-

cent to a given node. Interestingly, these symmetries are preserved in the presence of a large class of interaction potentials, including the Hubbard local interaction. The conserved quantum numbers associated to this symmetry are simply the parity of the total electron number in each Aharonov-Bohm cage. Because of this strong constraint, only pairs of electron can tunnel from one cage to another.

A first consequence, assuming that the local \mathbb{Z}_2 symmetry cannot be spontaneously broken, is that such a system is *never* a Landau Fermi liquid, since the single electron propagator is short ranged in space. This establishes a qualitative difference between \mathbb{Z}_2 networks and geometries such as the dice lattice. In the latter case, Aharonov-Bohm cages are no longer protected by a symmetry in the interacting system, and therefore a Fermi liquid induced by interactions seems perfectly plausible. This extends the distinction established for bosonic systems for which a single boson condensate is always destroyed on a \mathbb{Z}_2 network, whereas it survives on the dice lattice in spite of a large discrete ground-state degeneracy.

Using a simple mean-field analysis, completed by an unbiased renormalization group (RG) approach, we first conclude that no superconducting instability is expected, in spite of the particle pair hopping term generated by electron-electron interactions preserving the local \mathbb{Z}_2 symmetry. The RG analysis shows that long-ranged pair hoppings are generated at intermediate energies, but the typical hopping range remains of the order of the lattice spacing. This time, these results are in sharp contrast with the bosonic counterpart, where the absence of a single boson condensate leaves room for a perfectly stable boson *pair* condensate¹¹, with very interesting properties such as topological ground-state degeneracies¹³. The main result given by the RG is the presence of a strong coupling low-energy fixed point, dominated by the long-distance fluctuations of a local spin density wave order parameter. The appearance of this fixed point can be attributed to the presence of Aharonov-Bohm cages, since in the model considered here, independent links would behave as Luttinger liquids.

We should note that the RG calculation has been done on a simplified model, where all the lattice points inside a given Aharonov-Bohm cage are equivalent. So we have not incorporated the physics of Friedel density oscillation induced by the nodes, which are known to renormalize the single-electron scattering matrices at these nodes, as long as the system is in the one dimensional regime above the energy scale $h\nu_F/L$, which can be as large as a few Kelvin degrees in a GaAs/GaAlAs structure. The validity range of this simplified model has been formulated in terms of a very simple criterion on the value of the reflexion coefficient at the network nodes. It has to be low enough, otherwise, the disconnection induced by electronic scattering on Friedel density oscillations dominates over the tendency to build a SDW instability, and then, the low energy state appears to be a collection of

independent Luttinger liquid segments.

This study raises some open questions regarding the transport properties of such incoherent \mathbb{Z}_2 metal. It would be very interesting to compute the temperature dependence of the conductivity. At temperatures above the spin density wave instability, it is likely to exhibit a power-law behavior, with a presently unknown exponent. In the strong coupling regime, a gap for single electronic excitations is expected, so most likely, the temperature dependence of the conductivity will show an activated behavior. Another fascinating question is the transport through hybrid structures such as a series of a normal metal, a \mathbb{Z}_2 network, and a normal metal. Indeed, for driving voltages below the \mathbb{Z}_2 gap (of the order of $h\nu_F/L$), incoming (resp. outgoing) electrons will have a strong tendency to be injected (resp. emitted) in pairs, although the \mathbb{Z}_2 network is far from a superconducting state. Maybe the most direct way to demonstrate this strange phenomenon in such a poorly conducting system would be through shot noise measurements.

Acknowledgments

We wish to thank J. Dufouleur, G. Faini, and D. Mailly for giving us the motivation for this work, and for several useful discussions. We also thank J. Vidal for his comments on the manuscript. Financial support of the DFG in SP1073 is gratefully acknowledged.

APPENDIX A: SPIN DENSITY WAVE INSTABILITY ON A \mathbb{Z}_2 NETWORK

For the sake of simplicity, let us consider the Hubbard local interaction. For an infinite 1D system, we decouple

the interaction as:

$$U \left(\langle \psi_\uparrow^\dagger(x) \psi_\uparrow(x) \rangle \psi_\downarrow^\dagger(x) \psi_\downarrow(x) + \langle \psi_\downarrow^\dagger(x) \psi_\downarrow(x) \rangle \psi_\uparrow^\dagger(x) \psi_\uparrow(x) \right)$$

Let us assume that $\langle \psi_\tau^\dagger(x) \psi_\tau(x) \rangle = \tau \Delta \cos(2k_F x)$. In linear response theory, self-consistency determines the mean-field critical temperature T^* from the requirement $U\chi^{(0)}(2k_F, T^*) = 1$, where $\chi^{(0)}(q, T)$ is the static charge susceptibility of the non-interacting electron gas at wave-vector q and temperature T . Because $\chi^{(0)}(2k_F, T) = (h\nu_F)^{-1} \ln(aE_F/k_B T)$, where a is a numerical factor of order unity, the mean-field temperature T^* obeys a BCS relation:

$$k_B T^* = aE_F \exp\left(-\frac{h\nu_F}{U}\right) \quad (A1)$$

For a \mathbb{Z}_2 network, our starting point is Eq. (11). Again, we are looking for a \mathbb{Z}_2 invariant order parameter of the form: $\langle \psi_{i\tau}^\dagger(x) \psi_{i\tau}(x) \rangle = \tau \Delta_i(x)$. With such an order parameter, the quantum expectation value of Eq. (11) taken for a Hartree-Fock state is equal to $-U(\Delta_i(x) + \Delta_j(x))^2$. We see that choosing a uniform spin density wave order parameter $\Delta_i(x) = \Delta$ definitely lowers the system interaction energy, and we expect a mean-field transition temperature of the same order of magnitude as for the single infinite wire with a repulsive local interaction. Note that this transition is uniquely driven by the first two terms in Eq. (11), that is the intra and inter cage interaction. The last two terms, i.e. the cage exchange and the pair hopping processes do not play a role in stabilizing the spin density wave state. As seen in section IV in a more elaborate treatment, these last two terms have the effect to lower the critical temperature by comparison to the mean-field estimate.

* Electronic address: kkyrylo@lpthe.jussieu.fr

† Electronic address: sdusuel@thp.uni-koeln.de

‡ Electronic address: doucot@lpthe.jussieu.fr

¹ G. Timp, R. E. Behringer, E. H. Westerwick, and J. E. Cunningham, in *Quantum Coherence in Mesoscopic systems*, edited by B. Kramer (Plenum, New-York, 1991).

² S. Washburn, and R. A. Webb, *Rep. Prog. Phys.* **55**, 1311, (1992)

³ G. Timp, A. M. Chang, J. E. Cunningham, T. Y. Chang, P. Mankiewich, R. Behringer, and R. E. Howard, *Phys. Rev. Lett.* **58**, 2814, (1987)

⁴ S. Pedersen, A. E. Hansen, A. Kristensen, C. B. Sorensen, and P. E. Lindelof, *Phys. Rev. B* **61**, 5457, (2000)

⁵ D. Mailly, C. Chapelier, and A. Benoit, *Phys. Rev. Lett.* **70**, 2020, (1993).

⁶ W. Rabaud, L. Saminadayar, D. Mailly, K. Hasselbach, A. Benoît, and B. Etienne, *Phys. Rev. Lett.* **86**, 3124, (2001).

⁷ C. Naud, G. Faini, and D. Mailly, *Phys. Rev. Lett.* **86**, 5104, (2001)

⁸ J. Vidal, R. Mosseri, and B. Doucot, *Phys. Rev. Lett.* **81**,

5888, (1998)

⁹ J. Vidal, B. Doucot, R. Mosseri, and P. Butaud, *Phys. Rev. Lett.* **85**, 3906, (2000)

¹⁰ J. Vidal, P. Butaud, B. Doucot, and R. Mosseri, *Phys. Rev. B* **64**, 155306, (2001)

¹¹ B. Doucot and J. Vidal, *Phys. Rev. Lett.* **88**, 227005, (2002)

¹² I. V. Protopopov, and M. V. Feigel'man, *Phys. Rev. B* **70**, 184519, (2004)

¹³ L. B. Ioffe and M. V. Feigel'man, *Phys. Rev. B*, **66**, 224503 (2002).

¹⁴ S. E. Korshunov, *Phys. Rev. B* **63**, 134503, (2001)

¹⁵ S. E. Korshunov, and B. Doucot, *Phys. Rev. B* **70**, 134507, (2004)

¹⁶ S. E. Korshunov, *Phys. Rev. B* **71**, 174501, (2005)

¹⁷ J. Dufouleur, G. Faini, and D. Mailly, private communications

¹⁸ B. Doucot, M. V. Feigel'man and L. B. Ioffe, *Phys. Rev. Lett.* **90**, 107003 (2003).

¹⁹ B. Doucot, L. B. Ioffe and J. Vidal, *Phys. Rev. B* **69**,

214501, (2003)

²⁰ T. Kottos, and U. Smilansky, Phys. Rev. Lett. **79**, 4794, (1997)

²¹ S. Elitzur, Phys. Rev. **D 12**, 3978, (1975)

²² K. Kazymyrenko, and B. Douçot, Phys. Rev. **B 71**, 075110, (2005)

²³ C. L. Kane, and M. P. A. Fisher, Phys. Rev. Lett. **68**, 1220, (1992)

²⁴ D. Yue, L. I. Glazman, and K. A. Matveev, Phys. Rev. **B 49**, 1966, (1994)

²⁵ S. Lal, S. Rao, and D. Sen, Phys. Rev. **B 66**, 165327, (2002)

²⁶ J. Solyom, Adv. Phys. **28**, 201, (1979)

²⁷ S. Dusuel, F. Vistulo de Abreu and B. Douçot, Phys. Rev. **B 65**, 94505, (2002)

²⁸ Hyun C. Lee, P. Azaria and E. Boulat, Phys. Rev. **B 69**, 155109, (2004)